TABLE II

The relative ranking from largest to smallest values of optic axis dispersion by average, mode, and median values. The values are calculated on the basis of percentage of Schmidt net area of "dispersal" polygons determined by the optic axis measurements. See text for method.

Rank	By mode	By average percent of net area		By median percent of net area		By average rank
1	Shocked Coconino ss.	Sh. Coco. ss.	3.7	Sh. Coco. ss.	1.17	Sh. Coco. ss.
2	Ries granite	Ries gr.	1.5	KT-1 ss.	0.37	Ries gr.
3	100 KT-2 granite	KT-2 gr.	1.4	KT-2 gr.	0.27	KT-2 gr.
4	100 KT-1 sandstone	Con. meta. ss.	1.1	Ries gr.	0.21	KT-1 ss.
5	Antietam ss.	Ries gn.	0.98	Ries gn.	9.21	Ries gn.
6	Ries gneiss	KT-1 ss.	0.86	Holleford gr.	0.19	Wabar ss.
7	Washington Blue Quartz gneiss	Fordham gn.	0.57	*Wabar ss.*	0.19	*Holleford gr.*
8	Cheshire quartzite	Wabar ss.	0.48	Wash. B. Qtz. gn.	0.18	Wash. B. Qtz. gn.
9	Wabar ss.	*Holleford gr.*	0.35	Ches. qtzite	0.16	Ches. qtzite
10	*Holleford granite*	Ches. qtzite	0.25	Antietam ss.	0.14	Antietam ss.
11	Fordham gneiss	Wash. B. Qtz. gn.	0.22	Fordham gn.	0.10	Fordham gn.
12	Mylonite	Antietam ss.	0.19	Mylonite	0.05	Con. meta. ss.
13	Contact metamorphosed ss.	Unsh. Coco. ss.	0.14	Con. meta. ss.	0.04	Mylonite
14	Unshocked Coconino ss.	Glasf. cal. ss.	0.10	Unsh. Coco. ss.	0.04	Unsh. Coco. ss.
15	Glasford calcareous ss.	Mylonite	0.04	Glasf. cal. ss.	0.03	Glasf. cal. ss.

We are indebted to R. S. Dietz, C. P. Thornton, N. Short, E. M. Shoemaker, and T. E. Bunch for many of these samples.

The italics emphasizes the position of the lowest-ranked impact source in each category. The fourth column averages the rankings of the first three columns.

Frequency distributions based on an area size class for most of the sections measured are given in Figure 13. The histograms of the shocked specimens are skewed to higher area classes and are more spread out than are those of unshocked specimens. This characteristic is especially noticeable in the last histogram of the figure, which averages the histograms of the two groups and provides the smoothing effect to be expected from a larger number of readings. It would be difficult to decide on the basis of a single histogram of only 25 readings, such as that of the Cheshire quartzite, that the specimen had or had not been subjected to impact. However, by calculation of the average, mode, and median values, an almost perfect separation can be made between samples from impact and non-impact environments. The relative ranking from largest to smallest values of optic axis dispersion by the average, mode, and median values of the polygonal areas are shown in Table 2 for seven samples of impact origin and eight of non-impact origin. The fourth column averages the three rankings and supports the complete separation effected by the median values.

It should be mentioned that, as with the x-ray diffraction asterism findings, the relative ranking of the impact samples does not necessarily imply the same order of the intensity of the impact event, because the samples available were from random locations.

Gneisses and quartzites are difficult to separate from impacted rocks on the basis of the average and mode values; they also rank immediately below the median values of rocks displaying the mildest impact damage. The concentration into the small area classes of optic axis scatter of quartz grains from contact metamorphosed sandstone and mylonite is surprising in view of the impression of chaotic fragmentation seen in the thin sections. However, this difference is understandable in view of basic differences between these metamorphic processes and those of impact.

Thermal effects are essentially one-dimensional, in the direction of expansion or contraction, and

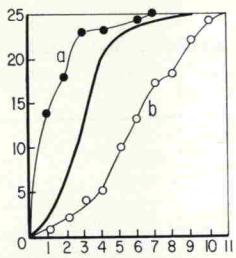

Fig. 14. A plot of the cumulative number of fractured or strained crystals of quartz whose optic axis dispersal polygons are equal to, or smaller than, the area specified on the abscissa. The numbers 1, 2, 3 etc., correspond to the percent of Schmidt net area divisions shown as abscissae in Figure 13. The lines (a) and (b) apply to the unshocked and shocked Coconino sandstone, respectively. The heavy line is the boundary which almost perfectly separates cumulative plots of non-shocked and shocked specimens, which, in general, also follow the descending order of Table 2.

are also slow, with a minimum of rotational components. Mylonitization processes are usually one-dimensional and relatively fast, with considerable rotation; but they occur at low pressures roughly equal to the shear strength of the rocks. The agencies of regional metamorphism which form gneisses, on the other hand, are long-acting, of low or high pressures depending on overburden, and are accompanied by shearing forces which act through large volumes and are variable with time and direction. The pressure environments produced by impacts are very rapid in development and impose pressures high enough to overcome the compressive, tensile, and shear strengths of both the massive rock and very often of its constituent minerals; in so doing shock processes become three dimensional and produce rotational tendencies. Furthermore, the attenuating rarefaction and compression waves impose additional opportunities for relative rotation of neighboring fragments.

An effective method of presenting the data is shown in Figure 14, where the cumulative number of grains displaying optic axis dispersal of a certain area or smaller is plotted against the area class. This diagram is based on the presentation of Dachille, Fauth, and Vand (1964). Results for unshocked and shocked Coconino sandstone (marked (a) and (b) in Fig. 14) indicate limits of plots obtained for the samples listed in Table 2. The heavy line between them is the boundary traced between plots of the two groups as separated by median and average rank in Table 2. The boundary is not perfect, because the upper parts of the plots for specimens of thermally metamorphosed sandstone and Fordham gneiss veered into high-area values. Nevertheless, points plotting well to the left or right of this boundary would strongly indicate a non-impact or impact history, respectively. For data plotting close to the boundary, curves with median values greater than that of the boundary would indicate an impact origin, particularly if the middle half of the cumulative curve were also to the right of the boundary.

In Figure 15 are shown the similar results from optic axis measurements of quartz grains in granodiorite from the Hardhat nuclear explosion site. The plots for the 13 kb and 32 kb locations practically coincide, as do those for 40 kb and 60 kb specimens. Unfortunately, thin sections of material exposed to higher pressures were not available at this time. However, sections of equivalent rocks from the Sedan cratering shot, subjected to shock pressures in excess of 150 kb, were examined and the results are also plotted. When compared with the boundary curve of Figure 14, cumulative curves for the Hardhat and Sedan specimens fall well to the right in the "shocked" area. By contrast, the curve of highly-deformed mylonite lies in the non-shocked side, well to the left of the boundary. Figure 15 demonstrates the potential utility of optic axis measurements in the field of shock metamorphism.

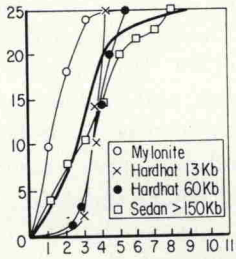

Fig. 15. Cumulative curves of quartz optic axis dispersion data of samples from the Hardhat and Sedan nuclear explosions, contrasted with data for a mylonite. The heavy line indicates the boundary discussed in Figure 14.